

One-dimensional x-ray imaging using a spherically bent mica crystal at 4.75 keV

J. Workman,^{a)} S. Evans, and G. A. Kyrala

Los Alamos National Laboratory, Box 1663, Mail Stop E-526, Los Alamos, New Mexico 87545

(Presented on 20 June 2000)

One-dimensional x-ray imaging of static gold bars using a spherically bent mica crystal is presented for the first time at an x-ray energy of 4.75 keV. X rays are produced using 1-ns-square pulses on the TRIDENT laser facility driving the He-like resonance transition in solid titanium disks. Time-integrated images of square profile parallel gold bars are recorded on direct exposure film with a magnification of ~ 10 . Rising edge measurements of the bars demonstrate resolutions of about 6–7 μm over a 400 μm field of view. © 2001 American Institute of Physics.
[DOI: 10.1063/1.1315648]

I. INTRODUCTION

An important diagnostic technique used with high-powered lasers for determining spatially and temporally resolved properties of high-density plasmas is x-ray imaging, both in self-emission and backlighting.¹ In particular, x rays have the penetration to determine plasma density and interface position and motion when inaccessible to optical probing. The denser and longer the plasma, the higher the x-ray energy required. Unfortunately, the production of high-energy x rays can require a significant fraction of the laser energy to be used in exciting these transitions.² This can lead to lower x-ray fluxes on the detector, and thus image quality degradation due to poor photon statistics.³ Future experiments at the National Ignition Facility (NIF) will require backlighters with minimum energies of several kiloelectron volts (keV).

Diagnostics must be designed to increase throughput and collection efficiency in order to maximize the low yields of high-energy x-ray sources. X-ray pinhole imaging is a standard diagnostic but requires high x-ray fluxes due to the low throughput. In addition, spatial resolution is ultimately limited by diffraction effects from the pinhole. For high x-ray energies, thick pinholes will limit the field of view. Alternatives to pinhole imaging include the use of x-ray collection optics made from grazing-incidence metal coating and multilayered mirrors.^{4,5} For accurate measurements of plasma density, a monochromatic x-ray source is required. Crystal spectrometers provide excellent energy-resolving power while, in addition, providing high spatial resolution when curved.^{6–10} Estimates of high x-ray throughput near normal incidence for spherically curved Bragg crystals demonstrate their potential as high-energy imagers in low-flux environments.¹¹

Spatial resolution is often limited by the x-ray detector, requiring high-magnification systems in order to use gated, streaked, or charged-coupled-device (CCD) electronic acquisition (typically, detector resolutions are from 20 to 100

μm). High magnification may also require even larger collection and throughput of the x-ray optical system than low-resolution systems. Recently, spherically curved x-ray crystals have been used to spatially resolve several-micron-scale features using framing cameras at high magnification at x-ray energies of 1–2 keV.¹² This article demonstrates the potential for one-dimensional high-spatial-resolution imaging from a simple crystal geometry at medium x-ray energies, specifically, at 4.75 keV.

X-ray crystals work on the principle of constructive interference in reflection from the crystal lattice for a given angle and x-ray energy. The angle at which a particular energy is reflected is described by Bragg's law as

$$n\lambda = 2d \sin(\Theta_B),$$

where n is the order of the reflection, λ is the x-ray wavelength, d is the crystal plane spacing, and Θ_B is the angle from the crystal plane at which the x rays are reflected. For mica crystals, it has been shown that for a single-crystal orientation, the high-order reflections can be quite pronounced. In fact, up to the 15th-order reflection has been measured in mica.¹³ It has also been shown that bent crystals can significantly increase the collection efficiency not only due to angle-matching conditions with increasing aperture but also due to a reduction in penetration depth.^{14,15}

II. EXPERIMENT

Imaging in these experiments was provided by a spherically bent concave mica crystal used in seventh order bent to a radius of curvature of 100 mm. Before bending, the crystal is cleaved along the (002) axis giving a $2d$ spacing of 19.84 Å. In seventh order, this allows reflection of the He-like resonance emission of titanium ($1s-2p^1P_1$) at 4.75 keV at an angle of 22.9° with respect to the crystal normal (Bragg angle of 67.1°). The deviation from normal incidence leads to astigmatism in the focal plane. Although two-dimensional imaging is possible without additional optics, at these larger incident angles the resolution would be quite poor. For curved crystals, placement of the x-ray source on the Rowland circle ensures the highest spectral resolution and closest

^{a)}Electronic mail: workman@lanl.gov

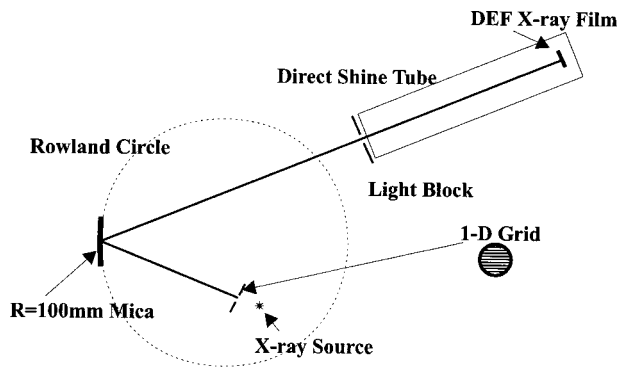


FIG. 1. One-dimensional $10\times$ x-ray microscope using a concave, spherically curved mica crystal. A one-dimensional grid of gold bars is imaged onto DEF x-ray film. The grid is oriented with bars running parallel to the paper.

matching to Bragg conditions across the crystal surface.¹⁶ This location is not always practical for magnifying systems where, as in Fig. 1, the source must be inside the Rowland circle. The object to be imaged was placed 8.5 mm from the point x-ray source with a ~ 1.5 mm aperture at the object plane. This aperture limits illumination of the crystal to an area of about one square centimeter. (Translation of the crystal reveals several areas with defects affecting image quality discussed below.) In reality, for this radius of curvature the width of the crystal, meridional plane (in the plane of Fig. 1), that matches the Bragg conditions is on the order of a millimeter due to the rocking curve and location of the source.¹⁰ The curvature of the crystal increases the area of the crystal matching the Bragg conditions. In the other axis, sagittal (perpendicular to the plane of Fig. 1), Bragg conditions are met along the entire height. The reason for the difference in matching conditions along the two axes is the geometry. Vertically (sagittally), the source is not displaced from the crystal center while horizontally (meridionally) the source is displaced. This means that changes in angle vertically follow the crystal radius while horizontally changes in angle do not follow the crystal radius. The crystal was arranged to provide one-dimensional imaging in the sagittal plane, maximizing the surface of the crystal used for focusing. The object was placed about 6 cm from the crystal to provide a magnification of $10\times$ when recording at a distance of ~ 60 cm. The intermediate focus in the meridional plane, as shown in Fig. 1, allowed placement of an aperture to minimize background and to stop direct optical and x-ray emission from the titanium x-ray source. A direct shine tube, as shown in Fig. 1, was also placed between the light block and film to minimize background. Object grids consisted of parallel gold bars of square profile. The bar width was $40\ \mu\text{m}$ and open space was $22\ \mu\text{m}$ with an overall period of $62\ \mu\text{m}$. A 10 mil Be filter was placed between the x-ray source and grid to prevent damage to the grid from ablated material. The crystal was protected by a 10 mil Be filter and the direct exposure film (DEF) film was filtered with 5 mil Be. The Bragg angle was set using a rotation stage with the normal defined by the focused reflection of a HeNe alignment laser back on itself. The Bragg angle was then fine tuned with the actual x-ray signal.

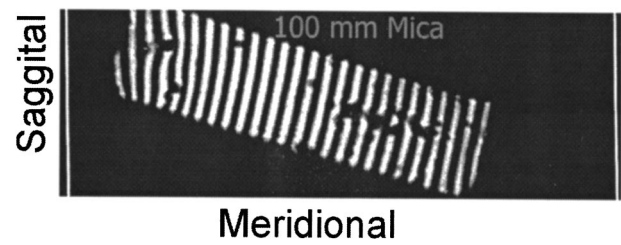


FIG. 2. Optical interferogram of 100 mm radius of curvature mica crystal used for 1D imager using a ZYGO. Crystal dimensions are approximately $1\times 5\ \text{cm}^2$.

Before using the mica crystal, an optical interferogram using a ZYGO was taken in order to determine regions where the crystal was not uniformly bent.¹⁷ This is only a measure of the surface quality and does not reflect any crystal imperfections. It was determined that the region just left of center in Fig. 2 was adequate for optical and possibly x-ray imaging. For the experiments the central one square centimeter region of the crystal was used. Evidence of the defects was observed in the x-ray images presented below but has not been rigorously correlated.

III. RESULTS

At the TRIDENT laser facility at Los Alamos National Laboratory 1-ns-square laser pulses, with energies around 100 J, were used to illuminate the front side of $25\text{-}\mu\text{m}$ -thick titanium disks at an irradiance of about $2\times 10^{15}\ \text{W}/\text{cm}^2$ at a wavelength of 527 nm.¹⁸ A flat crystal LIF (200) spectrometer was used to record time-integrated spectra for each shot, as shown in Fig. 3. Emission from the titanium disks is dominated by the He-like $1s^2-1s2p$ transitions at an energy of 4.75 keV. This backlighting source was placed 8.5 mm from the object grid in order to increase the illumination of the object.

Figure 4 shows the one-dimensional (1D) image of the $40\ \mu\text{m}$ gold bars obtained in a single laser shot. The energy dispersion of the mica crystal allows discrimination of the He and H-like emission lines. Imaging is in the vertical direction while astigmatism smears the image in the horizontal

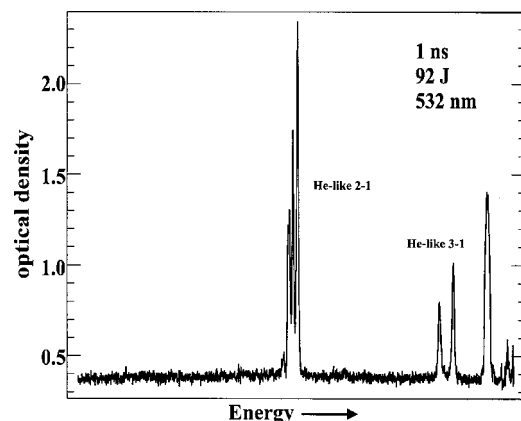


FIG. 3. Ti spectra, measured using a flat crystal (LIF) spectrometer for the x-ray backlighter. Incident laser intensity was near $2\times 10^{15}\ \text{W}/\text{cm}^2$. Emission is dominated by the He-like $1s^2-1s2p$ transitions.

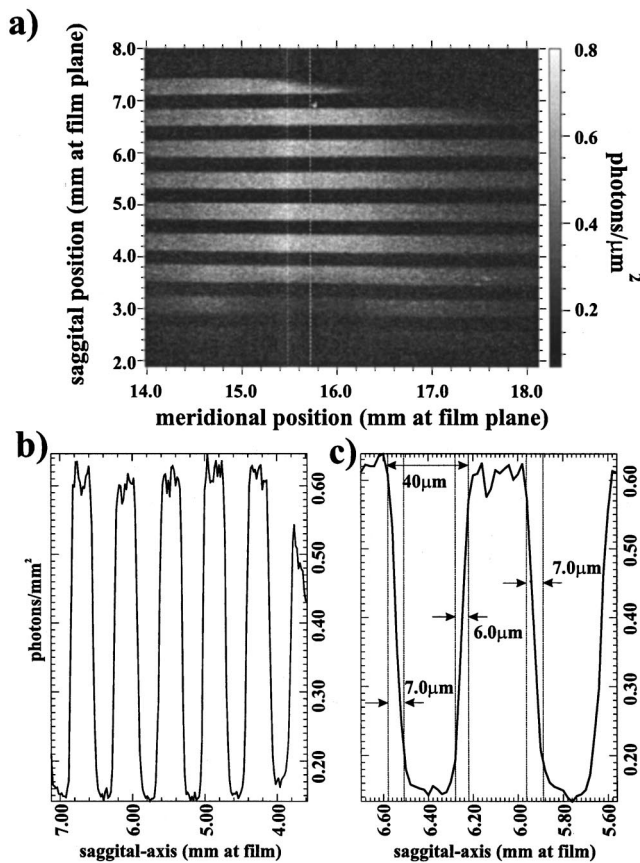


FIG. 4. (a) Digitized image of 62- μm -period 1D square profile parallel grid using a 10 \times magnification crystal microscope. Bar width is 40 μm and open width is 22 μm . (b) Lineout averaged over ten digitized units; the region scanned is indicated by the white lines in (a). (c) Lineout showing 6–7 μm resolution on the rising edge (10%–90%).

direction. Images were recorded on DEF and then digitized with 20 \times 20 μm^2 resolution. Optical density was converted to photons per square micron using calibration data from Henke *et al.*¹⁹ The tapered loss of the image on the top right is due to the direct shine tube used to block background. Near the bottom of Fig. 4(a) the image is obscured by a defect in the crystal. It is not clear whether this defect is correlated to any the defects seen in Fig. 2.

Figure 4(b) is an averaged lineout showing six bars, as indicated by the white rectangle in Fig. 4(a). Averaging was over 220 μm at the film plane, 11 digitized elements, corresponding to about 22 μm at the object plane. Figure 4(c) is a magnified view of two of the gold bars in Figs. 4(a) and 4(b). It should be noted that the region between the gold bars is not always consistent with the 22 μm spacing indicated by the 62 μm period. This is most likely due to stress in the mounting process, which can pull the bars away from each other. This irregular period was observed under a microscope. Measurements of the rising edges on the gold bars indicate 6–7 μm spatial resolution. These numbers are determined by measuring the rise from 10% to 90% of the transmission. The measurements were taken across the area indicated by the white rectangle in Fig. 4(a). The field of view across which the resolution was 6–7 μm was limited to about 400 μm by the light block, which obscured the image,

and the defect. Calibration of the spatial scale was determined by the 40 μm bar width and indicates a magnification of 9.5–10.

IV. DISCUSSION

Diffraction-limited focusing for an ideal configuration of our optical system would predict submicron resolution.²⁰ However, resolution can be degraded by several factors. These include the optical system (orientation and aperturing of the crystal and object), recording orientation, crystal quality, and the digitization process. Digitization at 20 μm in the image plane corresponds to about 2 μm digitization in the object plane. With 6–7 μm measured resolution this gives only about three elements with which to determine resolution. Rotation of the film with respect to the image plane will give a change in magnification across the film. Because the f number of the crystal imager is very large (order of 100), tolerances on the film position are not extremely sensitive. Crystal quality was not determined using x-ray diffraction, however, the surface quality was checked optically and indicated a reasonable surface. Orientation of the parallel gold bars with respect to the crystal is imperative for high-resolution imaging. In a one-dimensional imaging system a sharp edge will be degraded in the focusing direction as $L \sin \Theta$, where L is the length of the object being imaged and Θ is the misaligned rotation of the parallel bars. Over a 1 mm length, a half-degree rotation translates to almost 9 μm of optical blur in an edge. (In fact, the crystal does have some focusing power in the other axis, such that the rotation will not degrade the image as severely as stated above.) The rotation of the grid was not controlled accurately in these experiments.

In conclusion, a one-dimensional 10 \times magnification crystal imager using spherically bent mica has been constructed with demonstrated 6–7 μm spatial resolution at an x-ray energy of 4.75 keV. Determination of the spatial resolution was limited by the film digitization and object orientation. Higher magnification (20 \times) would resolve the digitization error, while careful alignment of the object rotation with respect to the crystal would improve the blur. While submicron diffraction-limited focusing is theoretically possible, mechanical constraints make 1 μm resolution a more realistic goal.

ACKNOWLEDGMENTS

The authors would like to thank A. Faenov for bending crystals, the TRIDENT operations crew, and B. Carpenter and Bechtel Nevada for film processing and digitization. This work was performed under the auspices of the U.S. Department of Energy under Contract No. W-7405-ENG-36.

¹B. A. Hammel, D. Griswold, O. L. Landen, T. S. Perry, B. A. Remington, P. L. Miller, T. A. Peyser, and J. D. Kilkenny, *Phys. Fluids B* **5**, 2259 (1993).

²R. Kauffman, in *Physics of Laser Plasma*, edited by A. Rubenchik and S. Witkowski (North-Holland, New York, 1991).

³A. Rose, *J. Opt. Soc. Am.* **43**, 715 (1953).

⁴F. J. Marshall and Q. Su, *Rev. Sci. Instrum.* **63**, 5080 (1992).

⁵J. H. Underwood, A. C. Thompson, J. B. Kortright, K. C. Chapman, and D. Lunt, *Rev. Sci. Instrum.* **67**, 1 (1996).

- ⁶B. A. Bryunetkin, S. A. Pikuz, I. Y. Skobelev, and A. Y. Faenov, *Laser Part. Beams* **10**, 849 (1992).
- ⁷T. A. Pikuz, A. Ya. Faenov, S. A. Pikuz, V. M. Romanova, and T. A. Shelkovenko, *J. X-Ray Sci. Technol.* **5**, 323 (1995).
- ⁸C. Brown *et al.*, *Phys. Plasmas* **4**, 1397 (1997).
- ⁹A. Ya. Faenov, I. Yu. Skobelev, S. A. Pikuz, G. A. Kyrala, R. D. Fulton, J. Abdallah, Jr., and D. P. Kilcrease, *Phys. Rev. A* **51**, 3529 (1995).
- ¹⁰J. Workman, T. Tierney, S. Evans, G. Kyrala, and J. Benage, Jr., *Rev. Sci. Instrum.* **70**, 613 (1999).
- ¹¹J. A. Koch *et al.*, *Appl. Opt.* **37**, 1784 (1998).
- ¹²Y. Aglitskiy *et al.*, *Appl. Opt.* **37**, 5253 (1998).
- ¹³S. A. Pikuz, V. M. Romanova, T. A. Shelkovenko, T. A. Pikuz, A. Ya. Faenov, E. Forster, J. Wolf, and O. Wehrhan, *Quantum Electron.* **25**, 16 (1995).
- ¹⁴D. Taupin, *Bull. Soc. Fr. Mineral. Cristallogr.* **87**, 469 (1964).
- ¹⁵G. Holzer, E. Forster, M. Gratz, C. Tillman, and S. Svanberg, *J. X-Ray Sci. Technol.* **7**, 50 (1997).
- ¹⁶E. Forster, K. Gabel, and I. Uschmann, *Laser Part. Beams* **9**, 135 (1991).
- ¹⁷ZYGO Corporation Middlefield, CT.
- ¹⁸N. K. Moncur, R. P. Johnson, R. G. Watt, and R. B. Gibson, *Appl. Opt.* **32**, 4274 (1995).
- ¹⁹B. L. Henke, J. Y. Uejio, G. F. Stone, C. H. Dittmore, and F. J. Fujiwara, *J. Opt. Soc. Am. B* **3**, 1540 (1986).
- ²⁰M. Born and E. Wolf, *Principles of Optics* (Cambridge University Press, New York, 1980).